Inorg. Chem. **2007**, *46*, 3996–4001

Hydrothermal Vanadium Fluoride Chemistry: Four New V^{3+} Chain Structures

David W. Aldous, Nicholas F. Stephens, and Philip Lightfoot*

EaStCHEM, School of Chemistry, University of St Andrews, St Andrews, Fife KY16 9ST, U.K.

Received October 27, 2006

An exploratory study of the hydrothermal chemistry of vanadium in HF solutions has resulted in the preparation of four new vanadium (III) fluorides with chainlike structural motifs. $[NH_4]_2[VF_5]$ (**1**) and $[C_2N_2H_{10}][VF_5]$ (**2**) feature infinite chains of trans corner-sharing $VF_4F_{2/2}$ octahedra, $[C_4N_2H_6][VF_5]\cdot H_2O$ (**3**) has cis corner-sharing $[VF_4F_{2/2}]_\infty$ chains, and $[C_{10}N_2H_8][VF_3]$ (**4**) has trans corner-sharing $[VF_2F_{2/2}]_\infty$ chains bridged into sheets by the 4,4′-bipy linker. All four compounds exhibit antiferromagnetic behavior.

Introduction

The combination of HF and an organic template or structure-directing agent (SDA) in hydrothermal synthesis is well known, with many phosphates and phosphonates in particular being discovered using this methodology.[1,2] Fluoride is often incorporated into the products of such reactions along with phosphate or other oxyanions. However, there has been surprisingly little work in such systems where fluoride represents the only anionic ligand. Several groups have recently begun to explore organically templated metal fluoride chemistry, and a variety of 2D and 3D structures have been reported in, for example, aluminum,[3−5] uranium,[6] zirconium,[7,8] beryllium,[9] scandium,[10,11] and yttrium[12] fluoride systems. A review focusing mostly on amine-templated oligomeric fluoro-anions of Mn, Fe, and Al has also been published.[13]

Although the structural chemistry of inorganic metal fluorides is well established,[14] the great range of organic species typically used as SDAs in hydrothermal chemistry would be expected to lead to a much wider range of metal fluoride crystal architectures than is currently known, as has been observed in the chemistry of metal phosphates during the past 20 years or so. Currently, we are exploring vanadium fluoride-based hydrothermal chemistry, and we have discovered a rich variety of organically templated oxyfluorides, generally containing V^{4+} in the form of the highly polar vanadyl (VO^{2+}) group.[15,16] Under some experimental conditions (which have not yet been fully elucidated), further reduction to V^{3+} can occur, in which case it appears more common to produce fully fluorinated vanadium centers, rather than oxyfluorides. The first examples of our explorations in this area are presented here. All four compounds exhibit chains of corner-sharing octahedral V^{3+} centers, linked via fluorine atoms. The structural characteristics and magnetic properties of these materials are described.

Experimental Section

Synthesis. $[NH_4]_2[VF_5]$ **1**, $[C_2N_2H_{10}][VF_5]$ **2**, $[C_4N_2H_6][VF_5]\cdot H_2O$ **3**, and $[C_{10}N_2H_8][VF_3]$ **4** were all synthesized hydrothermally. All of the products were made in 27 mL Teflon-lined stainless steel autoclaves and heated at 220 °C, 160 °C, 190 °C, and 160 °C

* To whom correspondence should be addressed. E-mail: pl@st-and.ac.uk.

(1) Férey, G. *J. Fluorine Chem*. **1995**, *72*, 187.
(2) Ouellette, W.; Yu, M. H.; O'Connor, C. J.; Zubieta, J. *Inorg. Chem.* **2006**, *45*, 7628.
(3) Harlow, R. L.; Herron, N.; Li, Z.; Vogt, T.; Solovyov, L.; Kirik, S. *Chem. Mater*. **1999**, *11*, 2562.
(4) Adil, K.; Goreshnik, E.; Courant, S.; Dujardin, G.; Leblanc, M.; Maisonneuve, V. *Solid State Sci.* **2004**, *6*, 1229.
(5) Loiseau, T.; Muguerra, H.; Marrot, J.; Férey, G.; Haouas, M.; Taulelle, F. *Inorg. Chem.* **2005**, *44*, 2920.
(6) Francis, R. J.; Halasyamani, P. S.; O'Hare, D.; *Chem. Mater*. **1998**, *10*, 3131.
(7) Bauer, M. R.; Ross, C. R.; Nielson, R. M.; Abrahams, S. C. *Inorg. Chem.* **1999**, *38*, 1028.
(8) Sykora, R. E.; Ruf, M.; Albrecht-Schmitt, T. E. *J. Solid State Chem*. **2001**, *159*, 198.
(9) Gerrard, L. A.; Weller, M. T. *Chem.—Eur. J.* **2003**, *9*, 4936.
(10) Stephens, N. F.; Slawin, A. M. Z.; Lightfoot, P. *Chem. Commun.* **2004**, 615.
(11) Stephens, N. F.; Lightfoot, P. *Solid State Sci*. **2006**, *8*, 197.
(12) Stephens, N. F.; Lightfoot, P. *J. Solid State Chem.* **2007**, *180*, 260.
(13) Bentrup, U.; Feist, M.; Kemnitz, E. *Prog. Solid State Chem*. **1999**, *27*, 75.
(14) Babel, D.; Tressaud, A. In *Inorganic Solid Fluorides;* Hagenmuller, P., Ed.; Academic Press: Orlando, FL, 1985. Massa, W.; Babel, D. *Chem. Rev.* **1988**, *88*, 275.
(15) Stephens, N. F.; Buck, M.; Lightfoot, P. *J. Mater. Chem.* **2005**, *15*, 4298.
(16) Aldous, D. W.; Goff, J. G.; Attfield, J. P.; Lightfoot, P. *Inorg. Chem.* **2007**, *46*, 1277.

10.1021/ic062061p CCC: $37.00
Published on Web 04/21/2007

Table 1. Crystallographic Data

	1	2	3	4
molecular formula	$[NH_4]_2[VF_5]$	$[C_2N_2H_{10}][VF_5]$	$[C_4N_2H_{12}][VF_5]\cdot H_2O$	$[C_{10}N_2H_8][VF_3]$
crystal system	orthorhombic	tetragonal	monoclinic	orthorhombic
space group	*Pnma*	*P*4/*ncc*	$P2_1/n$	*I*222
a (Å)	6.315(2)	12.837(2)	11.447(3)	3.797(4)
b (Å)	7.636(2)		5.910(2)	10.769(7)
c (Å)	10.921(4)	7.951(2)	13.880(6)	11.312(6)
β (deg)			91.54(2)	
V (Å^3)	526.6(3)	1310.1(4)	918.4(6)	462.6(6)
Z	4	8	4	2
total/unique reflns	3007/516	6977/593	6465/1936	3009/839
ind. reflns $>2\sigma(I)$	467	583	1612	713
fw	173.96	208.06	252.1	264.12
T (°C)	−180	−180	−123(2)	−123(2)
λ (Å)	0.7107	0.7107	0.8462	0.6709
ρ_{calcd} (g/cm^3)	2.30	2.11	1.81	1.90
R1 [$I > 2\sigma(I)$]	0.051	0.029	0.056	0.038
wR2 [$I > 2\sigma(I)$]	0.138	0.081	0.131	0.091

Table 2. Selected Bond Distances (Å), Angles (deg), and Bond Valence Sums (Σ, v.u.)

1	2	3	4
V1−F2 × 2 1.904(3)	V1−F1 × 4 1.908(1)	V1−F2 1.898(2)	V1−F1 × 2 1.842(2)
V1−F3 × 2 1.906(3)	V1−F2 × 2 1.9876(4)	V1−F3 1.901(2)	V1−F2 × 2 1.899(2)
V1−F1 × 2 2.005(1)	V2−F4 × 4 1.910(1)	V1−F5 1.908(2)	V1−N1 × 2 2.129(2)
	V2−F3 1.971(3)	V1−F4 1.935(2)	
V1−F1−V1 144.4(2)	V2−F3′ 2.004(3)	V1−F1′ 1.991(2)	
		V1−F1 1.999(2)	
		V1−F1-V1 162.0(1)	
∑(V1) 3.20	∑(V1) 3.20	∑ (V1) 3.18	∑ (V1) 3.48
∑ (F1) 0.88	∑ (V2) 3.18	∑ (F1) 0.91	∑ (F1) 0.69
∑ (F2) 0.58	∑ (F1) 0.57	∑ (F2) 0.59	∑ (F2) 1.18
∑ (F3) 0.58	∑ (F2) 0.92	∑ (F3) 0.58	
	∑ (F3) 0.90	∑ (F4) 0.53	
	∑ (F4) 0.57	∑ (F5) 0.57	

respectively. A general scheme for synthesis is as follows: 0.182 g (1.00×10^{-3} mol) of V_2O_5 was weighed into a 30 mL polypropylene bottle and dissolved with 0.5 mL (3.1×10^{-2} mol) of 48% HF at room temperature for 5 min. To the resultant solution, 5 mL (2.78×10^{-3} mol) of water was added (3 mL (1.67×10^{-3} mol) in the case of products 3 and 4) along with 5 mL (8.0×10^{-2} mol) of ethylene glycol, creating an orange solution. This solution was transferred to the autoclave, to which 3×10^{-3} mol of template was added (template for **1** = tris(2-aminoethyl) amine, for **2** = ethylenediamine, for **3** = piperazine, and for **4** = 4,4′-bipyridine). The reaction was then heated to the appropriate temperature for 24 h and allowed to cool to room temperature. The products were filtered, washed with water, and dried at 60 °C in air to give mid-green crystals for **1**−**3** and dark-green crystals for **4**. Elemental analysis, together with comparison of observed and simulated powder X-ray diffraction patterns, confirmed phase purity in each case (for **1**: H 4.17, N 15.20 (calcd H 4.43, N 15.39) revealing that the template had broken down in situ (see also ref 11 for a similar occurrence; for **2**: C 11.66, H 4.92, N 13.52 (calcd C 11.55, H 4.84, N 13.46); for **3**: C 18.42, H 5.08, N 10.45 (calcd C 19.06, H 5.06, N 11.10; for **4**: C 46.0, H 2.8, N 10.7 (calcd C 45.5, H 3.1, N 10.6).

Crystallography. Single-crystal X-ray diffraction data were collected with either a Rigaku Mercury CCD (for **1** and **2**) or a Bruker SMART system (for **3** and **4**) with silicon monochromated graphite monochromated Mo Kα or synchrotron radiation, respectively. All of the datasets were corrected for absorption via multiscan methods. The structures were solved by direct methods and refined by full-matrix least-squares techniques, using the SHELXS, SHELXL, and WinGX packages. The final models include anisotropic refinement for the non-hydrogen atoms and an isotropic riding model for the H atoms, except for **1**, where the H atoms were refined freely. Further details of the refinements are given in Table 1. For each structure, the oxidation state of vanadium was confirmed by bond valence sum analysis[17] in addition to the magnetic measurements.

Magnetic Measurements. Magnetic data were measured on a Quantum Design MPMS SQUID. Data were recorded in 5000 Oe field while warming the sample from 2 to 334 K in 4 K steps, following consecutive zero-field cooling (ZFC) and field cooling (FC) cycles. All of the data were normalized to the molar quantity of the sample, and any diamagnetic contributions were taken into consideration before data fitting.

Results and Discussion

Crystal Structures. Although there are a few examples of organically templated vanadium oxyfluorides,[15,16,18,19] there are no previously known examples of vanadium fluorides containing organic moieties and having extended −V−F−V− connectivity. Two examples of isolated $[VF_6]^{3-}$ octahedral units cocrystallizing with organocations are listed in the Cambridge database.[20,21] In addition, the compound $[enH_2][VF_5(H_2O)]$, presumably containing isolated $[VF_5(H_2O)]^{2-}$ units, is mentioned in Bentrup.[13] In each of our reactions, vanadium is reduced in situ under the reaction conditions used. Although further exploration of this phenomenon is

(17) Brown, I. D.; Altermatt, D. *Acta Crystallogr.* **1985**, *B41*, 244.
(18) Demsar, A.; Leban, I.; Giester, G. *Acta Chim. Slov.* **2002**, *49*, 259.
(19) Darriet, J.; Xu, Q.; Tressaud, A. *Acta Crystallogr.* **1987**, *C43*, 224.
(20) Silva, M. R.; Beja, A. M.; Paixao, J. A.; da Veiga, L. A. *Z. Kristallogr.* **2001**, *216*, 261.
(21) Silva, M. R.; Beja, A. M.; Paixao, J. A.; da Veiga, L. A. *Z. Kristallogr.* **2000**, *215*, 178.

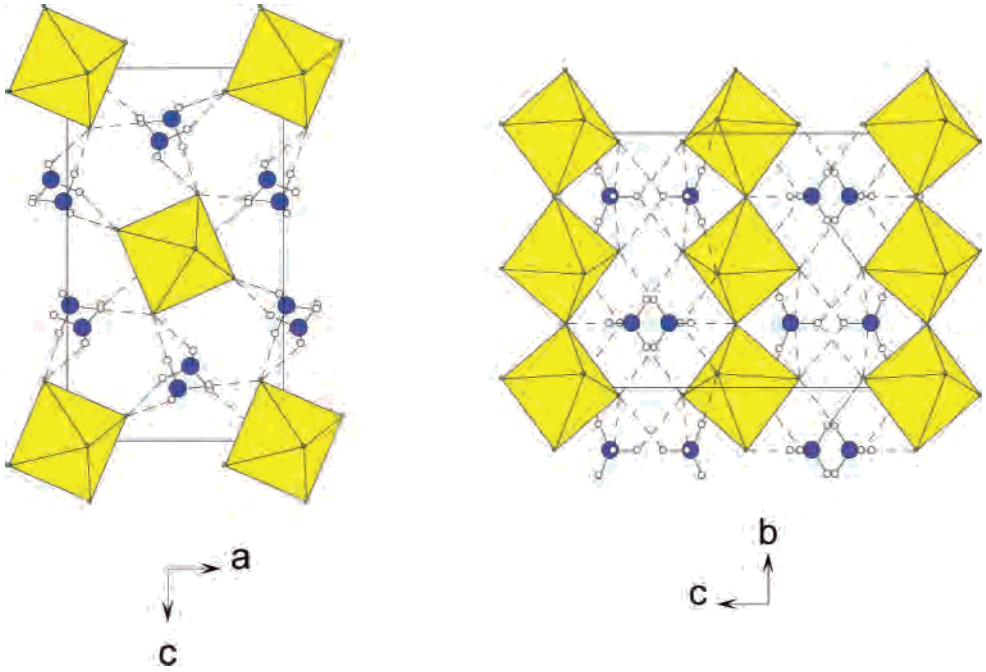

Figure 1. Views of **1** along the *b* and *c* axes showing isolated zigzag chains.

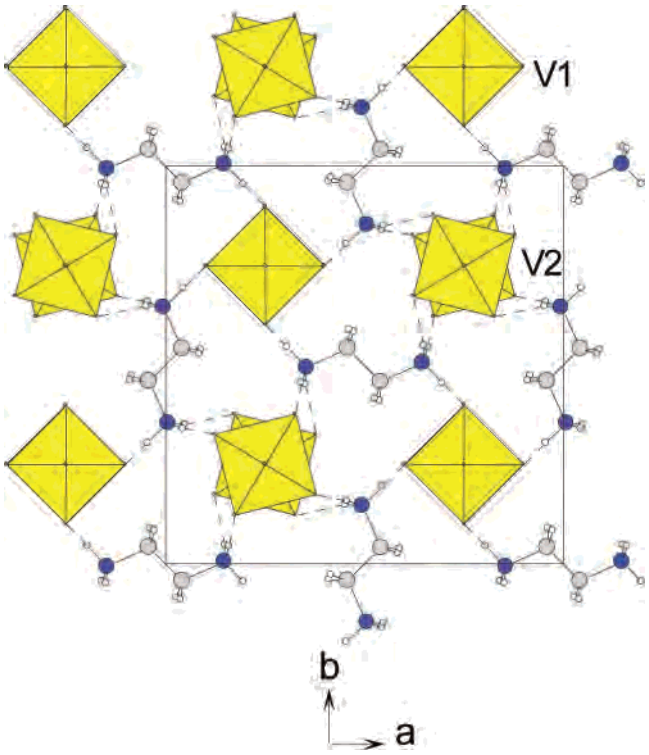

Figure 2. Structure of **2** viewed along the *c* axis, showing the eclipsed and staggered types of trans chain.

necessary, it is likely that the ethylene glycol present may act as a reducing agent.

The crystal structure of **1** exhibits infinite trans-connected zigzag chains of corner-sharing $[VF_4F_{2/2}]$ octahedra, which run along the *b* axis (Figure 1). The asymmetric unit comprises one V atom, which lies on an inversion center, two F atoms on general positions, and one F atom and two distinct NH_4^+ moieties on mirror planes. The V-centered octahedra are quite regular and display the expected lengthening of the bridging versus terminal V−F bonds. The nearest neighbor V−V interactions are 3.82 (intrachain) and 6.31 Å (interchain). Analogous chains are well known in metal fluoride chemistry,[12] occurring in the compositions $A^{II}M^{III}F_5$ (eg., $CaVF_5$) and $A^{I}_2M^{III}F_5$ (eg., $(NH_4)_2FeF_5$) and also in $MnVF_5(H_2O)_2$.[22] The NH_4^+ moieties are involved in substantial H bonding to the fluorine atoms (Supporting Information for all H bonding details). Selected bond lengths and angles for structures **1** to **4** are given in Table 2.

2 is isotypic with our previously reported scandium fluoride $[C_2N_2H_{10}][ScF_5]$[11] and also contains infinite trans vertex-sharing octahedral chains. In this case, there are two distinct V sites, which occur in eclipsed and staggered chains (torsion angle F−V−V−F between neighboring octahedra 28.2°), respectively, when viewed along the *c* axis (Figure 2). Both chains have V−F−V angles of 180°. H bonding from the template moiety occurs only to the terminal F atoms, F1 and F4, and not to the bridging atoms, F2 and F3, whose bond valences are satisfied by the intrachain bonding. As in **1**, there are no short-range magnetic interactions between neighboring chains: V−V = 3.98 (intrachain) and 6.42 Å (interchain).

The crystal structure of **3** contains cis-connected chains of $[VF_4F_{2/2}]$ octahedra which run along the *b* axis (Figure 3). The same type of chain has been observed in Rb_2CrF_5, $BaVF_5$, and VF_5.[14] In **3**, the chains are separated by the diprotonated piperazine moieties via a complex hydrogen-bonding network, which also incorporates a water molecule disordered over three sites within a channel along *b*. An alternative type of cis chain has also been observed in vanadium fluoride chemistry, viz., the zigzag-type chain in $SrVF_5$[23] (Figure 4). Among the known vanadium fluoride structure types, two further chain topologies are worthy of

(22) Leroux, F.; Mar, A.; Guyomard, D.; Piffard, Y. *Acad. Sci., C. R. Ser. II* **1995**, *320*, 147.

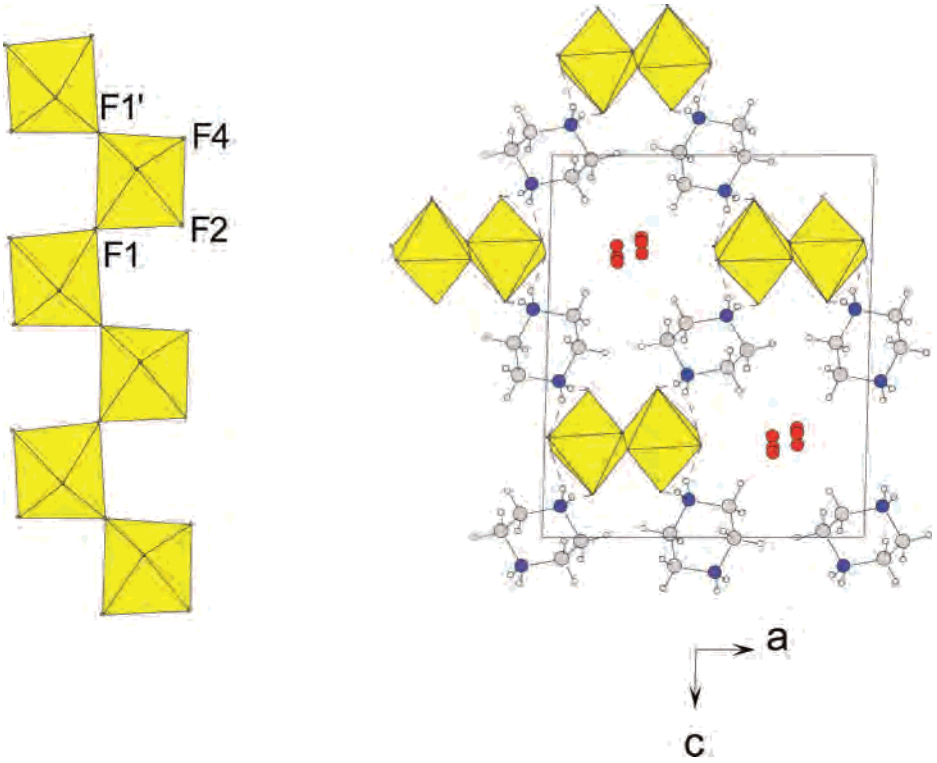

Figure 3. cis chain in **3** and the projection of the structure along *b*.

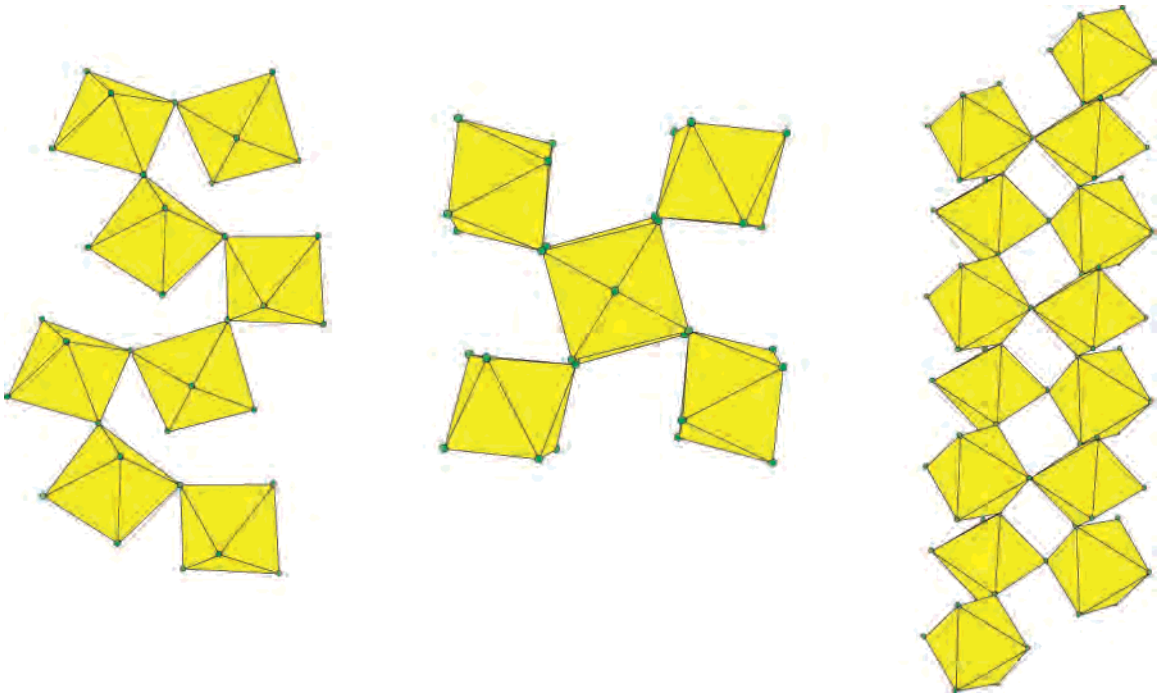

Figure 4. Previously observed vanadium fluoride chain topologies: (a) $SrVF_5$, (b) $BaVF_5$, and (c) $NaBaV_2F_9$.

mention: the branched chain in $BaVF_5$ ($BaFeF_5$ type[24]) and the stair-ladder type (composed of two linked cis-chains) of $NaBaV_2F_9$, which is reportedly isostructural with Ba_2CoFeF_9;[25] both of these are shown in Figure 4.

The crystal structure of **4** adds another dimension (literally) to the structural chemistry of vanadium fluorides. The single V atom is situated on a position of 222 symmetry and is octahedrally coordinated by a pseudo-square-planar array of atoms together with two axial N atoms from the 4,4′-bipy moiety. The octahedra share trans-F atoms to form $(VF_2F_{2/2}N_2)_n$ chains along the *a* axis (Figure 5). These chains are bridged by the bipy groups (which also lie on a 222 position) to form infinite metal-organic sheets in the *ac* plane (Figure 6). The

(23) Von der Muehll, R.; Daut, F.; Ravez, J. *J. Solid State Chem.* **1973**, *8*, 206.
(24) Georges, R.; Ravez, J.; Olazcuaga, R.; Hagenmuller, P. *J. Solid State Chem.* **1974**, *9*, 1.
(25) De Kozak, A.; Leblanc, M.; Samouel, M.; Férey, G.; de Pape, R. *Rev. Chim. Miner.* 1**981**, *18*, 659.

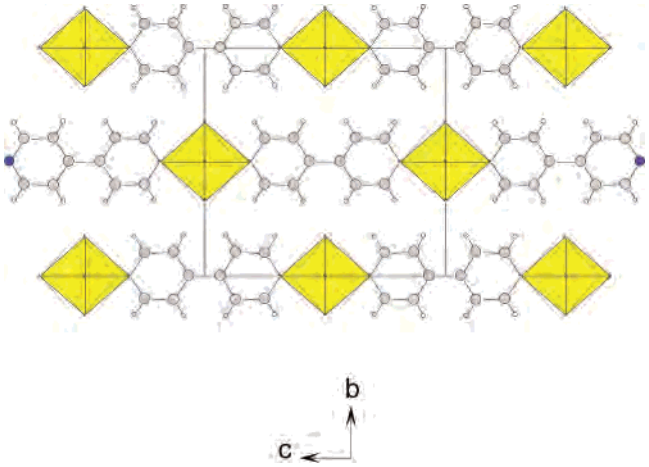

Figure 5. Structure of **4** along the *a* axis (chain direction), showing interchain bipy links to produce sheets in the *ac* plane.

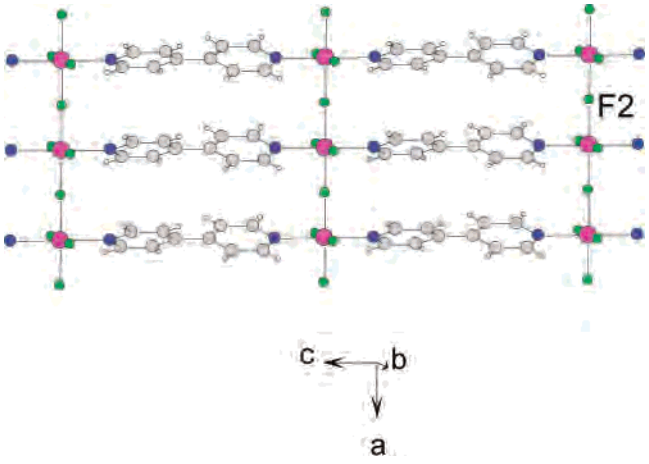

Figure 6. The vanadium fluoride-bipy layer in **4**.

Table 3. Magnetic Parameters from Curie−Weiss Fitting

	1	**2**	**3**	**4**
μ_{eff} (μ_B)	2.48(2)	2.82(1)	2.54(4)	1.92(7)
θ (K)	−19.9(5)	−121.9(3)	−67.1(6)	−4.73(3)
estimated T_N (K)	18	50	40	8

symmetry is lowered from *mmm* because of to the nonplanarity of the 4,4′-bipy moiety (torsion angle C2−C1−C1−C2 = 40.6(2)°). The V−F bonds in **4** are notably shorter than those in **1**−**3** perhaps because of the correspondingly weaker V−N bonding. There are short interchain C−H−F contacts from the bipy to the terminal F atoms of the neighboring chain (C2−H2−F1 = 3.19 Å), but these are not deemed to be energetically significant.[26]

In the case of **4**, the color of the sample, the vanadium bond valence sum, and the μ_{eff} value (below) may suggest a partial degree of oxidation, leading to mixed valence V^{3+}/V^{4+}. However, there is minimal crystallographic evidence for this; in particular, there is little evidence for the typical off-center displacement or short V═O length,[15,16] which would be expected to manifest itself in the atomic displacement parameters in the present model. The small anisotropy that does exist (for V, $U_{11} > U_{22} \approx U_{33}$) is suggestive that

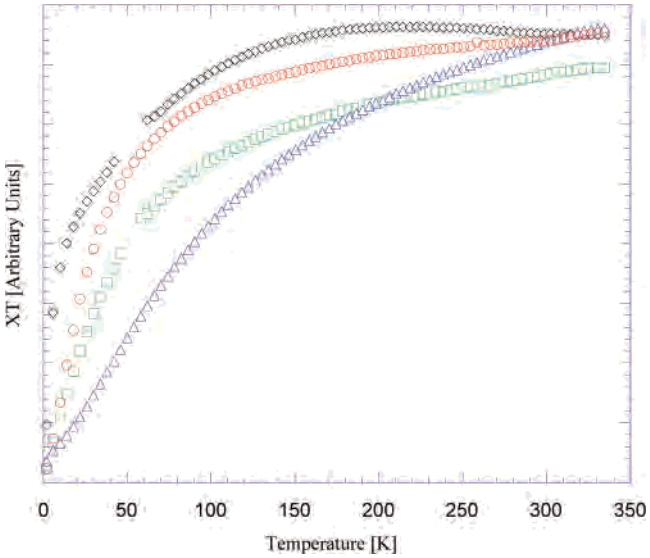

Figure 7. χT versus T for each of the samples, showing significant antiferromagnetic interactions in each case: ○ (**1**), △ (**2**), □ (**3**), and ◇ (**4**).

the bridging F2 site may be partially occupied by an oxide ion, which is also supported by the slightly high bond valence sum at this site. As a more direct probe of the vanadium oxidation state in **4**, we carried out an EPR experiment. EPR spectra for three samples are given in the Supporting Information: (i) **4**, (ii) $CsVOF_3$, which contains V^{4+} only (ref 16), and (iii) **3**, containing V^{3+} only. Unfortunately, because of the concentrated nature of the unpaired spins in these samples, the lineshapes are broad, and the fine structure expected for $S = {}^1/_2$ or 1 cannot be seen. However, there is sufficient similarity between spectra i and iii that we can suggest tentatively that **4** contains *predominantly* V^{3+}. Hence, we cannot rule out a partial mixed valence in **4**, but we have no definitive evidence for this.

Among the relatively few known examples of 2D metal halide−bipy arrays, most have edge-sharing chains of divalent metal chloride octahedra bridged by bipy.[27−29] In fact, as far as we are aware, the only known example of a metal fluoride−bipy coordination polymer is (4,4′-bipy)-$[MnF_3]$, which has the same framework topology as **4** but has a more complex modulated structure, which varies as a function of temperature,[30] a feature that has been ascribed to the Jahn−Teller nature of the Mn^{3+} cation. There is no evidence in **4** of similarly complex structural behavior, which is manifested in the Mn^{3+} derivative by anomalously anisotropic displacement parameters in the ideal *I*222 model.

Magnetic Susceptibilities. At high temperatures, the magnetic susceptibilities follow a Curie−Weiss law, and values of μ_{eff} (μ_B) and θ (K) were derived from this (Table 3). There are slight deviations from the spin-only value for V^{3+} (2.83μ_B), in particular in the case of **4**.

(26) Howard, J. A. K.; Hoy, V. J.; O'Hagan, D.; Smith, G. T. *Tetrahedron* **1996**, *52*, 12613.
(27) Hu, C.; Englert, U. *Angew. Chem., Int. Ed.* **2005**, *44*, 2281.
(28) Chippindale, A. M.; Cowley, A. R.; Peacock, K. J. *Acta Crystallogr.* **2000**, *56*, 651.
(29) Lawandy, M. A.; Huang, X.; Wang, R.-J.; Li, J.; Lu, J. Y.; Yuen, T.: Lin, C. L. *Inorg. Chem.* **1999**, *38*, 5410.
(30) Darriet, J.; Massa, W.; Pebler, J.; Stoef, R. *Solid State Sci.* **2002**, *4*, 1499.

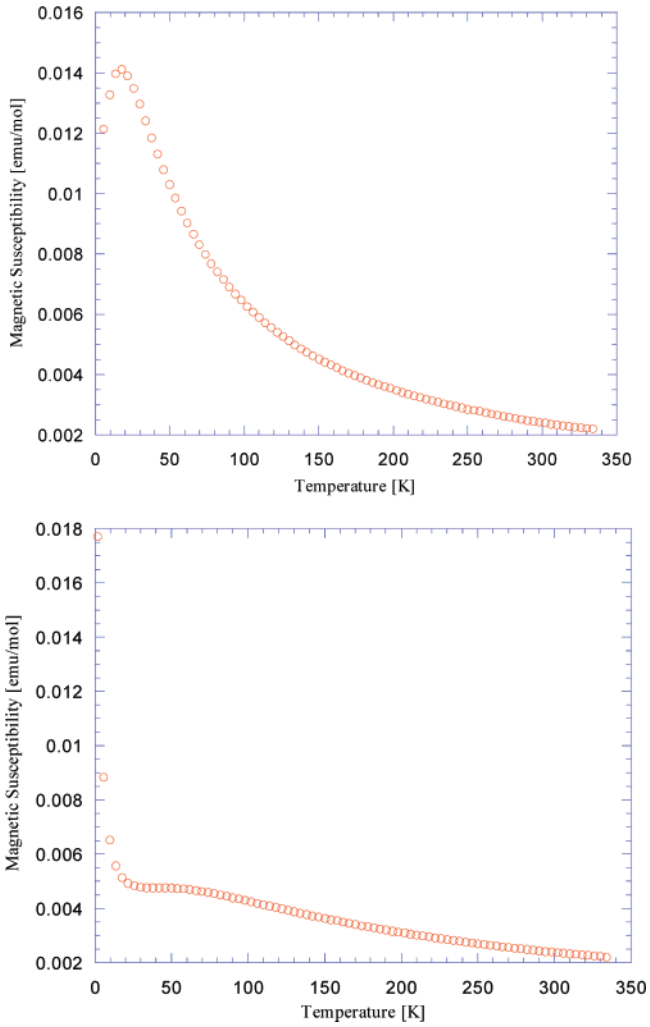

Figure 8. Raw $\chi(T)$ for **1** (above) and **2** (below).

The θ values reflect the presence of significant antiferromagnetic interactions in each case. Plots of χT versus T are shown in Figure 7. Each deviates from a constant value at low temperatures, again indicative of antiferromagnetic correlations, and the approximate Néel temperatures, T_N, given in Table 3 may be derived from the maxima of $d(\chi T)/dT$. In the case of **1** and **2**, broad maxima around T_N are clearly visible in the χ versus T plots (Figure 8), but for **3** and **4** these are weaker and are washed out by a sharp upturn in χ at low T because of a small amount of paramagnetic impurity (Supporting Information).

Conclusions

This preliminary exploration of the field of vanadium fluoride hydrothermal chemistry has revealed four different types of continuous V−F chains with corresponding magnetic phenomena, which may be described in simple terms as 1D antiferromagnetism. As is well known within hydrothermal chemistry in general, the factors affecting a given reaction outcome are complex and subtle. We have yet to establish control over the nature of the products formed in our systems. In particular, understanding of the factors controlling fluoride versus oxyfluoride formation, vanadium oxidation state, and dimensionality of the crystal structures are key targets that we continue to explore.

Acknowledgment. We thank Prof. Alex Slawin for assistance in collecting the diffraction data, Jason Farrell for help with the SQUID measurements, and Prof. John Walton for collecting the EPR data. We would also like to thank Dr. Richard Goff, Dr. Graham Smith, and Dr. D. Collison (EPSRC National EPR Service, Manchester. U.K.) for helpful discussions and the University of St Andrews and EPSRC for funding.

Supporting Information Available: ESR spectra, χ versus T plots, and CIF data. This material is available free of charge via the Internet at http://pubs.acs.org.

IC062061P